# Unravelling biotic versus abiotic processes in the development of large sulfuric-acid karsts

D. Laurent, G. Barré, C. Durlet, P. Cartigny, Cédric Carpentier, G. Paris, Pauline Collon, J. Pironon, E.C. Gaucher

*Geology*(G50658): 1–17, 2023
10.1130/G50658.1

# Unravelling biotic vs. abiotic processes in the development of large sulfuric acid karsts

Dimitri Laurent[1], Guillaume Barré[2,3], Christophe Durlet[4], Pierre Cartigny[5], Cédric Carpentier[1], Guillaume Paris[6], Pauline Collon[1], Jacques Pironon[1], and Eric C. Gaucher[3,7]

[1]*Université de Lorraine, CNRS, GeoRessources laboratory, F-54000 Nancy, France*
[2]*Département de géologie et de génie géologique, Université Laval, Québec, QC G1V 0A6, Canada*
[3]*TOTAL, Scientific and Technical Center Jean Féger, 64000 Pau, France*
[4]*Biogéosciences, CNRS, Université Bourgogne Franche-Comté, 21000 Dijon, France*
[5]*Université de Paris, Institut de Physique du Globe de Paris, CNRS, 75005 Paris, France*
[6]*Centre de Recherches Pétrographiques et Géochimiques, CNRS, Vandoeuvre-lès-Nancy, France*
[7]*University of Bern, Institute of Geological Sciences, CH-3012 Bern, Switzerland*

**Abstract** In carbonate rocks, natural production of sulfuric acid can form large karstic cavities. Where both epigenic and hypogenic speleogeneses have taken place, these processes are challenging to constrain, especially if there is more than one source of sulfur involved. Thanks to an innovative approach coupling geomorphology with measurements of multiple sulfur, oxygen and strontium isotopes, the present study of two French Pyrenean caves quantifies the relative influence of both microbial and thermochemical processes implied in sulfuric acid production. Multiple sulfur isotopes reveal that sulfate speleothems derived from a mixing of microbial $H_2S$ in hydrothermal water and fossil thermochemical $H_2S$ previously trapped within the cave host rock. We quantify the percentages of biotic and abiotic sulfuric acid speleogenesis that have taken place in these caves, paving the way for similar studies of other sulfuric acid caves, where only microbial activity was usually considered.

## 1 Introduction

Sulfuric acid speleogenesis (SAS) is known to create large karstic rooms in only a few thousands of years, one to two orders of magnitude faster than the "classical" epigenic karstic systems that form by meteoric and soil-derived carbonic acid (De Waele et al., 2016). Hence, sulfuric acid is one of the most powerful weathering agents of carbonate rock (e.g. Hill, 1987; Audra et al., 2009; D'Angeli et al., 2019a, b). In karst, sulfuric acid may be produced by three main processes: (i) oxidation of $H_2S$ derived from microbial sulfate reduction (MSR; Machel, 2001), (ii) oxidation of sulfide minerals (Morehouse, 1968; Tisato et al., 2012; Metzger et al., 2015), and (iii) oxidation of abiotic $H_2S$ produced from thermochemical sulfate reduction (TSR) (Laurent et al., 2021). These processes can all be active contemporaneously in a single karst setting, but their distinction and respective influence using geomorphological and conventional geochemical criteria are challenging. Sulfuric acid dissolution of carbonate rocks leads to the precipitation of sulfates (Hill, 1987):

$$H_2SO_4 + CaCO_3 + H_2O \rightarrow CaSO_4 \cdot 2H_2O + CO_2 \qquad (1)$$

Even if major sulfur isotope compositions ($^{32}S$ and $^{34}S$) of sulfate speleothems are good proxies to characterize the sulfur cycle in caves (e.g. Hill, 1987; Bottrell et al., 2001; Wynn et al., 2010; Temovski et al., 2018), they are not enough to determine source types and mixing of those types. But, although rarely applied in karst investigations (Zerkle et al., 2016; Laurent et al., 2021), multiple sulfur isotopes (MSI, $^{33}S/^{32}S$ and $^{34}S/^{32}S$) (Farquhar et al., 2007) can provide such information. In this paper, we combined MSI with strontium and oxygen isotopes, mineralogy and geomorphology, to quantify the biotic and abiotic contributions in SAS in two caves in the French Pyrenees.

## 2 Settings and methods

The Nébélé and Azaleguy caves are located in the Arbailles basin (northwest Pyrenees, France), a half-graben bordering the Aquitaine Basin. This basin formed during Jurassic and Early Cretaceous extensional phases, accompanied by diapirism of Triassic evaporites (James and Canérot, 1999; Fig.1a). The Nébélé Cave network extends more than 24 km within the Dogger carbonate formations capped by the impermeable Oxfordian Hosta marls (Fig.1a). Its speleogenesis started during the Late Pliocene along the Ithé valley, leaving the valley and cave systems perched after Pleistocene uplift (Vanara, 2000). The cave can be subdivided into two parts (Fig.1b): (i) the -100 m fossil level, between -85 and -120 m from the entrance; and (ii) the deeper active level (-145 to -177 m), with a general flow to the northeast up to the Uthurbietta resurgence. The Azaleguy Cave is also located along the Ithé valley, forming a 700 m-long, N-S oriented and 30°-inclined tunnel cave. It develops within an Albian marly limestone lens, 5 km southward of the Nébélé Cave entrance (Fig.1b). Both caves exhibit a high content of sulfate concretions potentially linked to the SAS process. In addition, in-situ gas analyses of the cave host rock reveal a significant content of $H_2S$ (> 200 ppmv; Fig.1A for location), suggesting a potential role in SAS. Methodology, detailed maps and multiple-S ($\delta^{33}S$ and $\delta^{34}S$), Sr ($^{87}Sr/86Sr$) and oxygen ($\delta^{18}O$) isotope values on minerals, thermo-mineral springs, and sulfate speleothems are available in the GSA Data Repository.

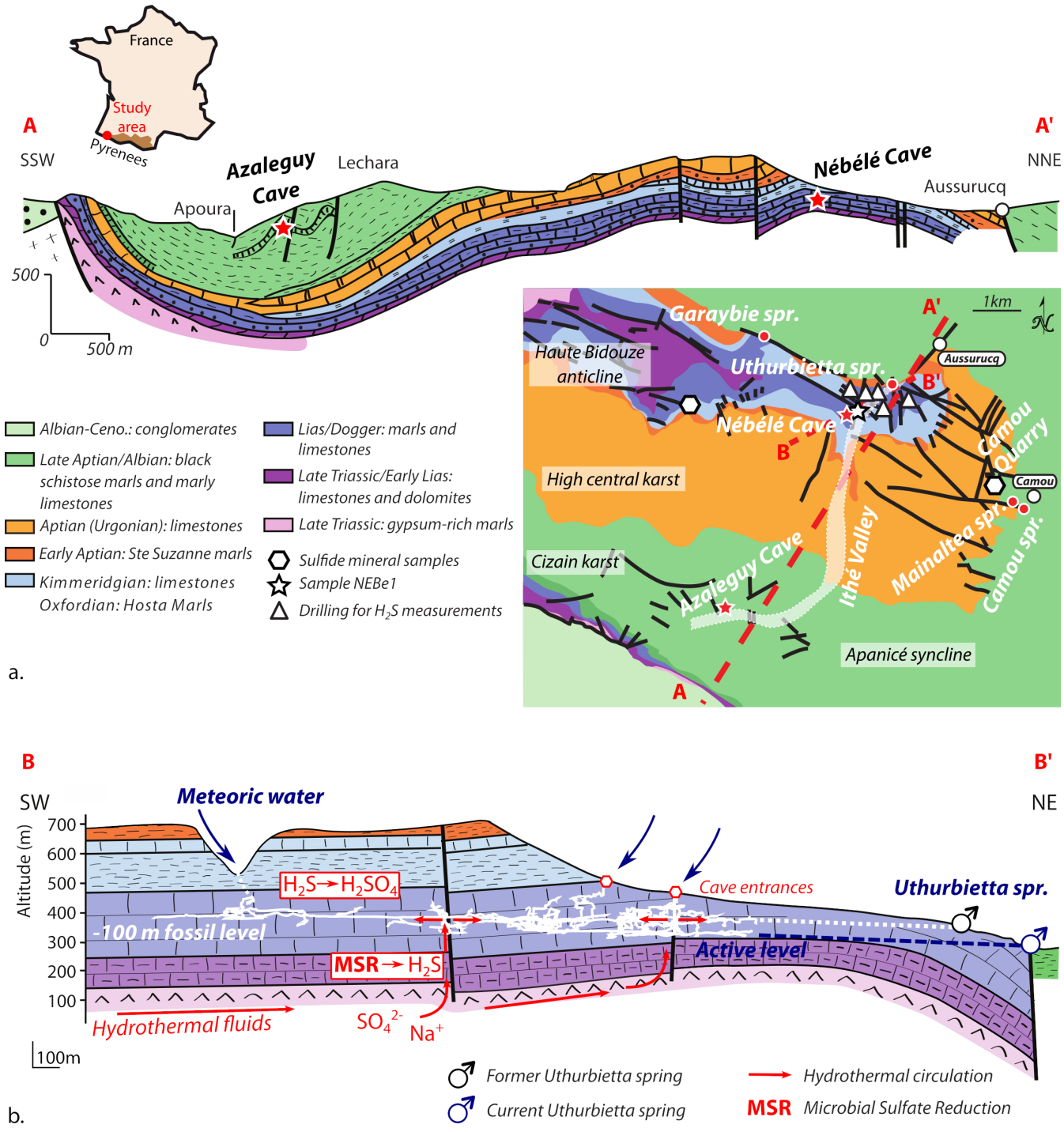


**Figure 1** a. NE-SW cross section and geological map with studied site locations. b. SW-NE cross section of the Haute Bidouze anticline showing the Nébélé Cave architecture and the regional hydrothermal fluid flow.

## 3 Sulfur cycle inferred from the origin of cave sulfates

Along the Nébélé Cave fossil level, and more particularly in the Scrouitch gallery (Fig.2a & b), Diffuse Reflectance Infrared Fourier Transform spectroscopy and X-Ray Diffraction on 10 samples of cave sulfate minerals reveal by order of abundance:

1. gypsum ($CaSO_4 \cdot 2H_2O$), forming dm-thick saccharoid crusts on cave walls (Fig.2c), cm-long efflorescences along small fissures, styloliths, and bedding planes (Fig.2d), and pluri-cm to m-long stalactites (Fig.2e), stalagmites, soda straws and helictites on the ceilings and floors;
2. sodium sulfate minerals, with thenardite ($Na_2SO_4$; Fig.2f), mirabilite ($Na_2SO_4 10H_2O$; Fig.2g), and blödite ($Na_2Mg(SO_4)_2 \cdot 4H_2O$), developed on the clayey floors, where they form flowers of fibrous crystals up to 50 cm-long.

Cave gypsum $\delta^{34}S$ values range between -26.44 and -20.20‰ with $\Delta^{33}S$ values between -0.009 and +0.009‰, and $\delta^{34}S$ values of sodium sulfates vary between -21.98 and -18.69‰ with $\Delta^{33}S$ values of -0.002‰ (Fig.3).

The Azaleguy Cave also hosts a significant amount of gypsum speleothems, precipitated in Aptian $H_2S$-rich marly limestones, and characterized by $\delta^{34}S$ values between -34.82 and -19.60‰, and $\Delta^{33}S$ values between -0.049 and +0.040‰

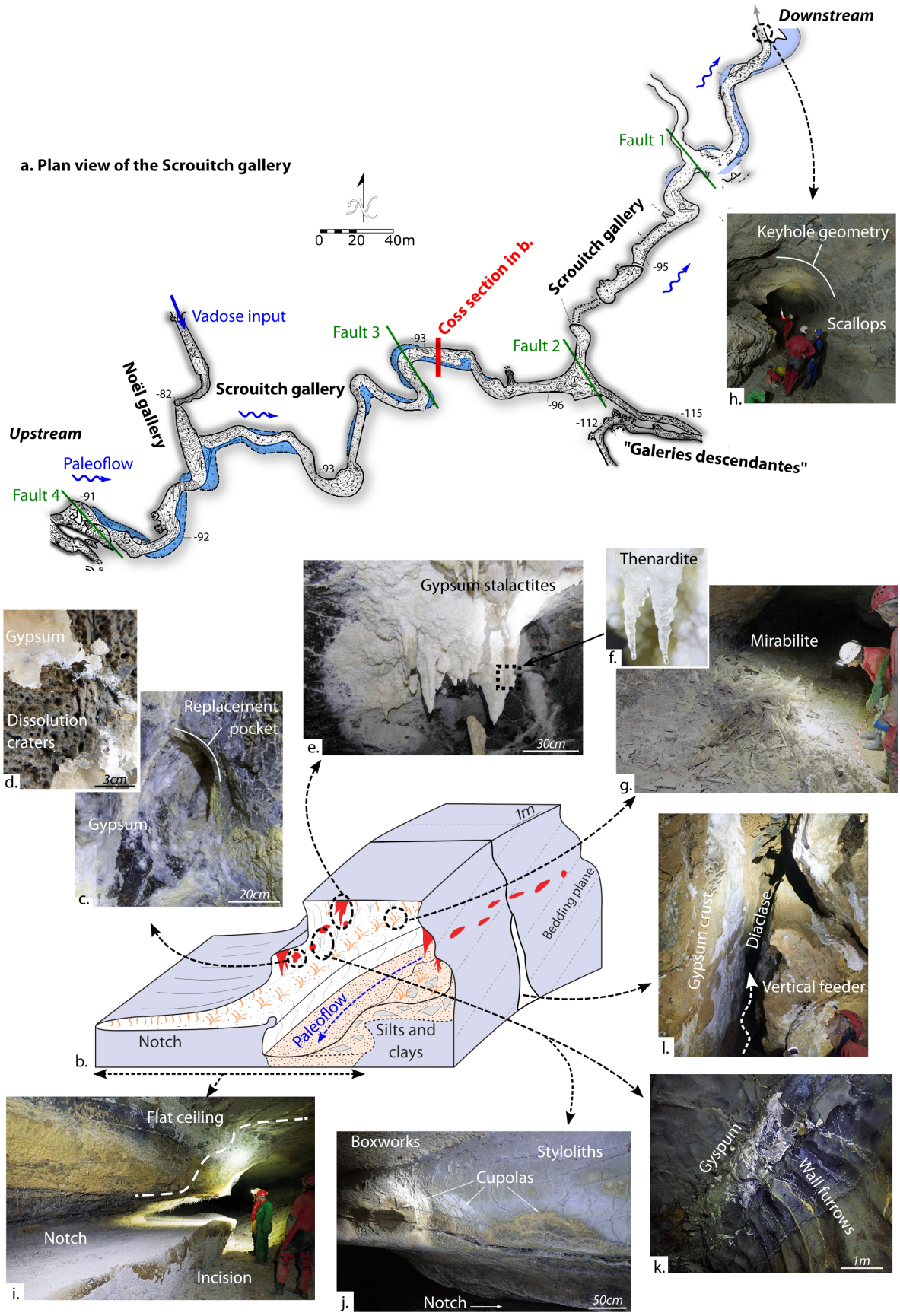


**Figure 2** a. Detailed topography of the Scrouitch gallery (modified from the Collectif Nébélé) with the position of horizontal notches in blue. Negative values correspond to the depth in meter relative to the cave entrance. b. General morphology and cave sulfate mineral distribution of the Scrouitch gallery. c. Massive gypsum crust resting on a replacement pocket. d. Small dissolution craters with gypsum efflorescences. e. Gypsum stalactites and crusts. f. Thenardite at the end of the stalactites. g. Giant flowers of mirabilite. h. Epigenic keyhole geometry and paragenetic scallops on cave walls. i. Perched deeply incised lateral notches. j. Cupolas affecting a cave wall above a lateral notch, and boxworks on the ceiling. k. Sub-vertical corrosion furrows on the cave wall. l. cm to dm-thick gypsum crust coating a large fissure.

(Fig.3).

In both caves, sulfide minerals are not present in sufficient quantity in the host rock (< 1wt%) to account for such a large amount of sulfate speleothems through their oxidation. Sulfide mineral oxidation from surrounding formations (Liassic and Aptian) can also be discarded as pyrites and chalcopyrites show very different MSI signatures ($\delta^{34}S$ values between -2.18 and +3.89‰, and $\Delta^{33}S$ values between -0.005 to +0.162‰; Fig.3) compared to that of cave sulfates, since sulfide oxidation only induces a low S fractionation (between 0.7‰ and 4.2‰; Findlay et al., 2019). The overlying Hosta marls and the Nébélé Cave clays (Fig.1b) are very poor in sulfur-bearing minerals and can also be excluded as significant S sources.

Our MSI results unambiguously follow a convex hyperbolic $\delta^{34}S - \Delta^{33}S$ relationship (Fig.3), typical of a mixing trend between two sulfur pools, which thus induces $^{33}S$-depleted mixing products (Ono et al., 2006). Such a correlation between measured and modelled data is unique and illustrates the high potential of MSI to decipher the sulfur cycle in caves.

The $H_2S$ dissolved in the Mainaltea mineral spring close to Nébélé Cave (Fig.1a) corresponds to the most $^{34}S$-depleted end member (-45.54‰ in summer; -54.35 and -53.90‰ in winter) showing high $\Delta^{33}S$ values (+0.111‰ in summer; +0.179 and +0.192‰ in winter), typical of MSR (Farquhar et al., 2007; Johnston, 2011). The known source for sulfate ions used for MSR are Triassic evaporites, which are only recognized at depth (Vanara, 2000). Abnormally high temperature and high dissolved sulfate content are evidenced in surrounding thermo-mineral springs (Fig.1a): the Garaybie spring (T = 15°C against 11°C in nearby rivers); and the Camou hot spring (28 < T < 38°C, and 1180 mg/l of sulfate ions), both of which confirm the migration of deep high-temperature fluids in the area of the Nébélé Cave. MSI values of dissolved sulfate in Camou spring ($\delta^{34}S = +14.55$ and $\Delta^{33}S = -0.046$) are close to the signature of Triassic evaporites ($\delta^{34}S = +16.61$‰ and $\Delta^{33}S = +0.003$ ‰; analysed in the Caresse quarry, 40 km north of the Nébélé Cave). $\delta^{18}O$ values of Nébélé Cave gypsum (between +10.1 and +15.6‰ V-SMOW), as well as the $^{87}Sr/86$Sr values of sulfate minerals in both caves (Nébélé: between 0.700757 and 0.708200; Azaleguy: between 0.707287 and 0.707328), are also close to the Triassic seawater signature ($\delta^{18}O$ value of 13±2.8‰ V-SMOW – Crockford et al., 2019; $^{87}Sr/86$Sr values between 0.707273 and 0.707297 – Koepnick et al., 1990). As sulfate minerals were specifically found close to large-scale faults in both Nébélé and Azaleguy caves, low temperature hydrothermal fluids probably circulate per ascensum through these regional structures (Fig.1b). An abnormally high temperature above 15°C measured in the atmosphere of the whole Nébélé Scrouitch gallery, while other parts of the cave as well as surrounding caves at the same altitude are at c.a. 11°C, is also consistent with a hydrothermal influence.

The most $^{34}S$-enriched end-member corresponds to $H_2S$ in the host rock (content of 320 ppmv; measured by EA-IRMS). Thermal-desorption at 400°C was not enough to extract this $H_2S$, while no fluid inclusion was found within the scarce calcite veins. Therefore, $H_2S$ is likely trapped within the porosity of the rock (even if we do not exclude the influence of $H_2S$-rich calcite veins; Bahnan et al., 2021), and only released during dissolution. This trapped $H_2S$ shows $\delta^{34}S$ values between +13.29 and +16.29‰ and $\Delta^{33}S$ values between -0.002 and +0.018‰, similar to the Triassic evaporite signatures. When all sulfates are reduced by TSR, the produced $H_2S$ has the same MSI signature than the initial sulfate (Worden and Smalley, 1996). This is fully consistent with TSR documented in the area (Biteau et al., 2006), and with previous suggestion for $H_2S$ resulting from complete TSR within Pyrenean Jurassic rocks (Barré et al., 2019).

Sulfate minerals of Nébélé and Azaleguy caves display S-isotope compositions consistent with the two end-members mixing curve (Fig.3), with relative influence of 41% and 59% respectively from TSR-derived and MSR-derived $H_2S$. It confirms the action of sulfuric acid through $H_2S$ oxidation, associated with the carbonate substitution by sulfate precipitation during progressive dissolution. A carbonate-sulfate substitution front is commonly considered either as inexistent in SAS (Spötl et al., 2021) or very thin (only 1 mm-thick; Plan et al., 2012), as the sulfate-carbonate substitution rate is higher than the invasion rate of sulfuric acid. However, Laurent et al. (2021) argued that the replacement front can penetrate up to a cm deeper into the host rock. In the Nébélé Cave, this front is also evidenced by negative $\delta^{34}S$ values between -15.10 and -14.60 ‰ of trace sulfates up to 3 cm depth from the gypsum interface (GSA Data Repository).

These ranges of $\delta^{34}S$ values for cave sulfate minerals are similar to many SAS studies (e.g. Hill, 1987; Hose et al., 2000; De Waele et al. 2016; Temovski et al., 2018), in which sulfuric acid production was suggested to be only related to microbial activity, thus possibly distorting the quantification of $H_2S$ fluxes if another $H_2S$ source is involved.

## 4 Synthesis and perspectives

Geomorphological observations and multiple-S, O, and Sr isotope data reveal a multiphase history that shaped the sulfuric caves in this region. Three speleogenesis time periods can be defined:

- (t1): We interpret that the Late Pliocene was a time of karstification mainly derived from meteoric water circulating in phreatic conditions (evidenced by paragenetic carving; Fig.2h, 4-t1), and responsible for the formation of the upper karstic levels (between -85 and -120 m), including the Scrouitch gallery. This configuration was like the currently active deeper karstic levels of the Nébélé Cave (Fig.1a). The MSI signature of sulfate ions in current Uthurbietta resurgence ($\delta^{34}S = +9.64$‰ and $\Delta^{33}S$ = -0.031‰) plots on the same MSR-TSR mixing interval as cave sulfate minerals and shows that 94% of the total 18.4 mg/l of sulfate ions were derived from oxidation of TSR-derived $H_2S$ in the host rock (Fig.3). The $H_2S$ amount was probably diluted during high water discharge and the sulfuric acid produced during the $H_2S$ oxidation only enhanced the epigenic process in phreatic conditions. According to MSI results, microbial influence on $H_2S$ production was limited at this time;

- (t2): The main widening phase of the Scrouitch gallery occurred during the progressive drop of the water table and the establishment of a meandering vadose river in the cave (Fig.4-t2), as evidenced by incised lateral deep notches perched 1.5 m above the current floor (Fig.2b and i). These notches crosscut the bedding plane strictly parallel to the floor (with a 0.7% gradient). Notches result from an acid water level, with intense dissolution effects at the water-atmosphere interface where atmospheric $O_2$ reacts with $H_2S$ to produce

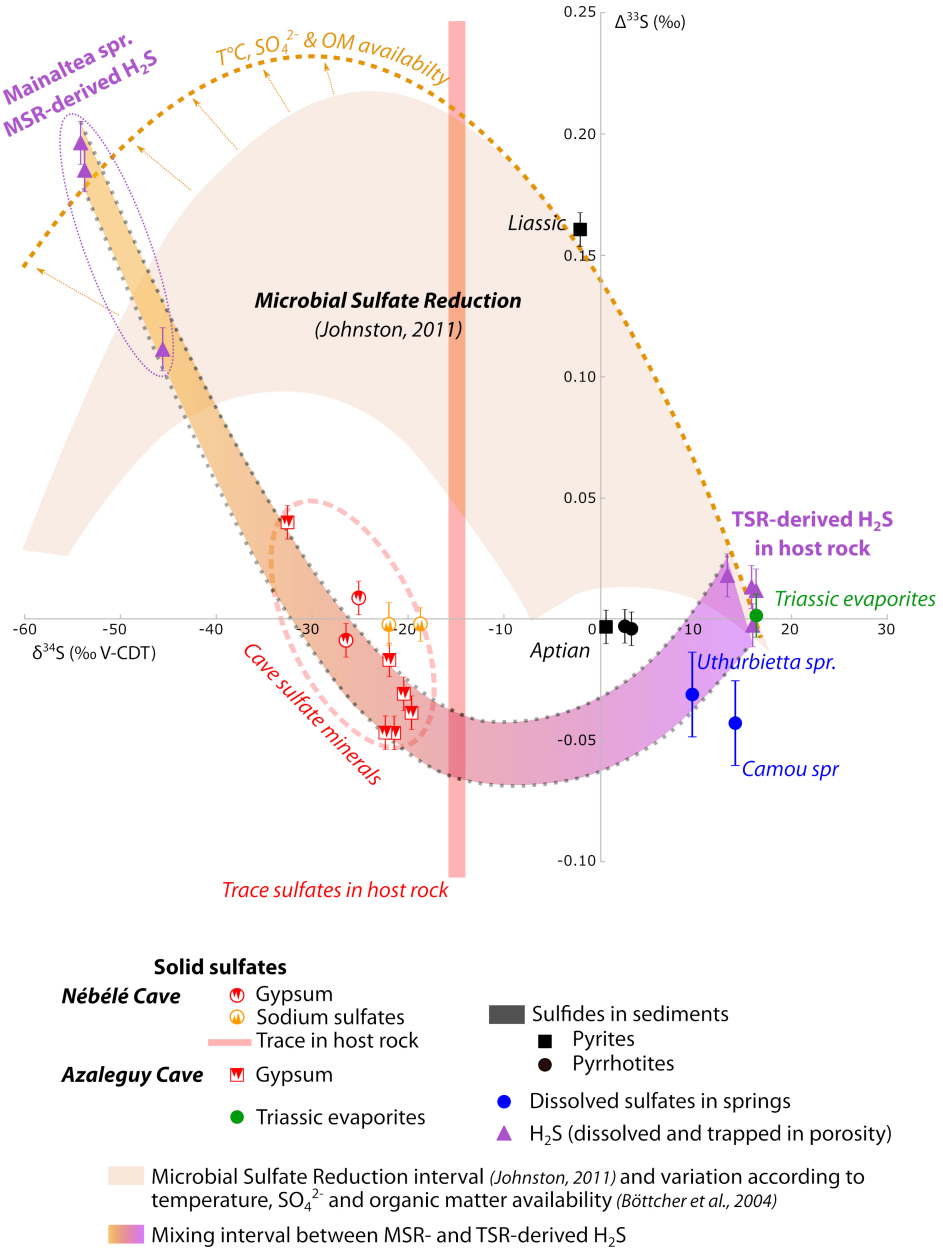


**Figure 3** Multiple sulfur isotopes diagram with all the sulfur species implied in the sulfate precipitation of both the Nébélé and Azaleguy caves.

sulfuric acid (Audra et al., 2009; De Waele et al., 2016). As the water standing in the passages is warmer than the rock temperature, it can evaporate and condense on the walls, favouring the condensation-corrosion process and the TSR-derived $H_2S$ extraction from the rock porosity. Condensation-corrosion phenomenon is visible in the cave through parietal morphologies affecting walls and ceiling (Fig.2) (e.g. Klimchouk, 2007; Audra et al., 2009; De Waele et al., 2016; Laurent et al., 2021): pluri-cm replacement pockets coated by gypsum crusts, pluri-dm symmetrical cupolas, boxworks with pseudomorphs of gypsum, pendants drip holes, 10 to 30 cm-deep vertical furrows extending from the gallery ceiling to the top of the notches, and gypsum coated fissures. SAS-related sulfate minerals formed in response to vadose condensation-corrosion processes. In these subaerial conditions, microbial activity can develop, with MSI revealing that the $H_2S$ used for sulfuric acid production was c.a. 50/50 derived from: (i) the in-situ MSR of Triassic sulfate ions conveyed by hydrothermal fluids, and (ii) the release during dissolution of the previously trapped TSR-derived $H_2S$ (Fig.3);

- (t3): The last and still active phase is the abandonment of the Scrouitch gallery by water flow during the Pleistocene regional base-level drop (Fig.4-t3) (Vanara, 2000). Water flows about 70 m deeper in galleries formed by the same karstic process of the first phreatic phase (t1) for the fossil level. Low-rate dissolution and sulfate precipitation in the fossil level continue at present through the diffuse condensation-corrosion processes (induced by air circulation), that oxidize the TSR-derived $H_2S$.

Our study also questions the role of SAS in the atmospheric carbon cycle, as sulfuric acid dissolution of carbonate rocks leads to $CO_2$ emissions in the atmosphere (e.g. Berner and Berner, 1996; Calmels et al., 2007). The SAS-related $CO_2$ budget has never been explored, mainly due to the difficulty

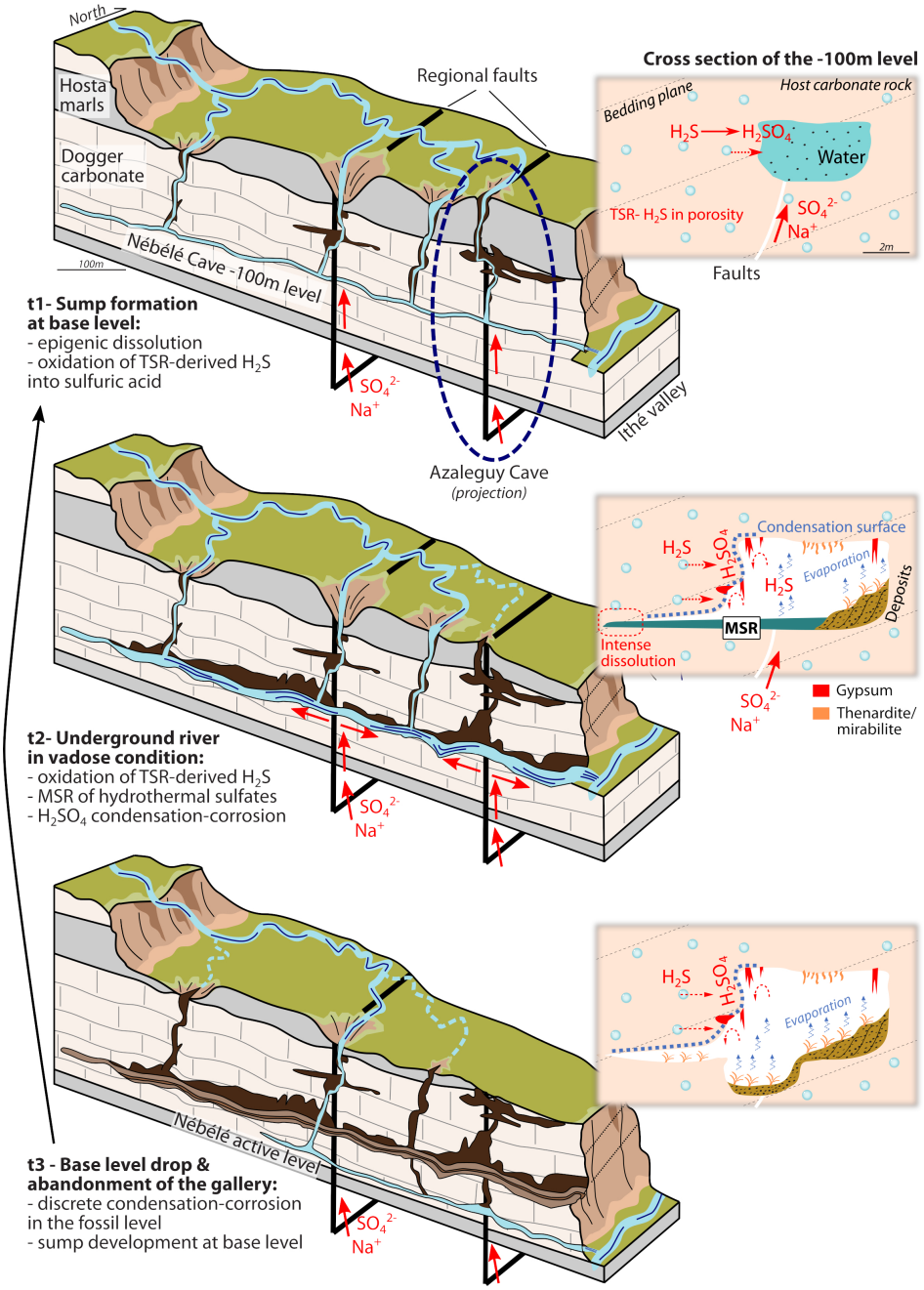


**Figure 4** Schematic MSR-TSR mixed SAS chronological model at the scale of the Nébélé network (left), with the projection of the fossil Azaleguy Cave, and at the scale of the Scrouitch gallery (right).

of identifying/quantifying the origin of sulfuric acid. For the Northern Pyrenees, we roughly calculated the $CO_2$ flux that SAS processes could have emitted by considering a 200 m-thick $H_2S$-rich Jurassic formation for a total area of 9000 $km^2$, a dissolution rate of 94 $m^3/km^2/yr$ during the last 407 kyr (Vanara, 2000), and a uniform intensity of SAS (details on calculation in GSA Data Repository). The resulting $CO_2$ flux of 33.9 t $CO_2$/yr over the last 407 kyr is certainly overstated. However, it demonstrates the relevance to extend worldwide such an approach, especially in caves affecting limestones which have trapped $H_2S$ in their matrix. As for the Arbailles basin, such $H_2S$-rich limestones are common across the Pyrenees (Bahnan et al., 2021), but also in other basins where TSR has occurred (e.g. Worden and Smalley, 1996; Cheng et al., 2022).

Finally, the originality of this work is the integration of $\Delta^{33}S$ measurements with other geochemical proxies more classically used in karst studies. In the future, this MSI method would be useful in quantifying multiple origins of sulfuric acid involved in the dissolution of deep-buried carbonate rocks that may have high potential for water and other economic resources.

## Supplemental Material

Suplemental material includes : Details of sampling, cave morphology and minerals, extended description of the data and methods, the data table of isotopic analyses, and details of the $CO_2$ budget calculation. Available freely on HAL, or here https://doi.org/10.1130/G50658.1

## Acknowledgements

This work was funded by TOTAL EP R&D (Pau, France) at CREGU (Nancy, France). We are grateful to D. Bartier and O. Barres for their technical support with XRD and DRIFT anal-

yses at GeoRessources lab (Nancy). We thank S. Revillon for strontium isotope measurements at IUEM (Plouzané, France). The Collectif Nébélé, P. Audra (Polytech Lab, Nice), D. Cailhol (INRAP) and J-Y. Bigot (AFK), are greatly thanked for their support during the different exploration phases.

## References

Audra P., Mocochain L., Bigot J.-Y., and Nobecourt J.-C, 2009, Morphological indicators of speleogenesis: hypogenic speleogens: in Klimchouk A. and Ford D.C. (Eds.), Hypogene speleogenesis and karst hydrogeology of artesian basins, Ukrainian Institute of Speleology and Karstology, Simferopol, Special Paper 1: 17-22.

Elias Bahnan, A., Pironon, J., Carpentier, C., Barré, G. and Gaucher, E.C., 2021, The diagenetic history of the giant Lacq gas field, witness to the apto-albian rifting and the Pyrenean orogeny, revealed by fluid and basin modeling: Marine and Petroleum Geology, 105250.

Barré, G., Elias-Bahnan, A., Motte, G., Ducoux, M., Hoareau, G., Laurent, D., and Gaucher, E. C., 2019, Hydrothermal fluid circulations in the western Pyrenees: new data on stable isotopes, in-situ gas analysis and fluid inclusions: E3S Web of Conferences, Vol. 98, p. 01001.

Berner, K.E., and Berner, R.A., 1996, Global Environment: Water, air and geochemical cycles: Upper Saddle River, New Jersey, Prentice Hall, 376 p.

Biteau, J. J., Le Marrec, A., Le Vot, M., and Masset, J. M, 2006, The aquitaine basin: Petroleum Geoscience, 12(3), p. 247-273.

Böttcher, M. E., Hespenheide, B., Brumsack, H. J., and Bosselmann, K., 2004, Stable isotope biogeochemistry of the sulfur cycle in modern marine sediments: I. Seasonal dynamics in a temperate intertidal sandy surface sediment: Isotopes in Environmental and Health Studies, 40(4), p. 267-283.

Bottrell, S. H., Crowley, S., and Self, C., 2001, Invasion of a karst aquifer by hydrothermal fluids: evidence from stable isotopic compositions of cave mineralization: Geofluids, 1(2), p. 103-121.

Calmels, D., Gaillardet, J., Brenot, A., and France-Lanord, C., 2007, Sustained sulfide oxidation by physical erosion processes in the Mackenzie River basin: Climatic perspectives: Geology, 35(11), p. 1003-1006.

Cheng, Y., Feng, Z., Guo, C., Chen, P., Tan, C., Shi, H., and Luo, X., 2022, Links of Hydrogen Sulfide Content With Fluid Components and Physical Properties of Carbonate Gas Reservoirs: A Case Study of the Right Bank of Amu Darya, Turkmenistan: Frontiers in Earth Science, 10, 910666.

Crockford, P. W., Kunzmann, M., Bekker, A., Hayles, J., Bao, H., Halverson, G. P., Peng, Y., Bui, T. H., Cox, G. M., Gibson, T. M., Wörndle, S., Rainbird, R., Lepland, A., Swanson-Hysell, N. L., Master, S., Sreenivas, B., Kuznetsov, A., Krupenik, V., and Boswell, A. W., 2019, Claypool continued: Extending the isotopic record of sedimentary sulfate: Chemical Geology, 513, p. 200-225.

D'Angeli, I.M., Nagostinis, M., Carbone, C., Bernasconi, S.M., Polyak, V.J., Peters, L., McIntosh, W.C., and De Waele, J., 2019a, Sulfuric acid speleogenesis in the Majella Massif (Abruzzo, Central Apennines, Italy): Geomorphology, 333, p. 167–179.

D'Angeli, I. M., Parise, M., Vattano, M., Madonia, G., Galdenzi, S., and De Waele, J., 2019b, Sulfuric acid caves of Italy: A review: Geomorphology, 333, 105-122.

De Waele, J., Audra, P., Madonia, G., Vattano, M., Plan, L., d'Angeli, I. M., Bigot, J.-Y., and Nobécourt, J.-C., 2016, Sulfuric acid speleogenesis (SAS) close to the water table: examples from southern France, Austria, and Sicily: Geomorphology, 253, p. 452-467.

Farquhar, J., Johnston, D. T., and Wing, B. A., 2007, Implications of conservation of mass effects on mass-dependent isotope fractionations: Influence of network structure on sulfur isotope phase space of dissimilatory sulfate reduction: Geochimica et Cosmochimica Acta, 71(24), p. 5862-5875.

Findlay, A. J., Boyko, V., Pellerin, A., Avetisyan, K., Guo, Q., Yang, X., and Kamyshny Jr, A., 2019, Sulfide oxidation affects the preservation of sulfur isotope signals: Geology, 47(8), p. 739-743.

Hill, C. A., 1987, Geology of Carlsbad cavern and other caves in the Guadalupe Mountains, New Mexico and Texas: Bull. 117, New Mexico Bureau of Mines and Minerals Resources, 162p.

Hose, L. D., Palmer, A. N., Palmer, M. V., Northup, D. E., Boston, P. J., and DuChene, H. R., 2000, Microbiology and geochemistry in a hydrogen-sulphide-rich karst environment: Chemical Geology, 169(3-4), p. 399-423.

James, V., and Canérot, J., 1999, Diapirism and post-triassic structural development of the western Pyrenees and southern Aquitaine (France): Eclogae Geologicae Helvetiae, 92(1), p. 63-72.

Johnston, D. T., 2011, Multiple sulfur isotopes and the evolution of Earth's surface sulfur cycle: Earth-Science Reviews, 106(1-2), p. 161-183.

Klimchouk, A.B., 2007, Hypogene Speleogenesis: Hydrogeological and Morphogenetic Perspective: National Cave and Karst Research Inst., Carlsbad, United States 106p.

Koepnick, R.B., Denison, R.E., Burke, W.H., Hetherington, E.A., and Dahl, D.A., 1990, Construction of the triassic and Jurassic portion of the Phanerozoic curve of seawater 87Sr/86Sr: Chem. Geol. Isot. Geosci. Sect. 80, p. 327–349.

Laurent, D., Durlet, C., Barré, G., Sorriaux, P., Audra, P., Cartigny, P., Carpentier, C., Paris, G., Collon, P. Rigaudier, T., Pironon, J., and Gaucher, E.C., 2021, Epigenic vs. hypogenic speleogenesis governed by H2S/CO2 hydrothermal input and Quaternary icefield dynamics (NE French Pyrenees): Geomorphology, 387, 107769.

Machel, H. G., 2001, Bacterial and thermochemical sulfate reduction in diagenetic settings—old and new insights: Sedimentary Geology, 140(1-2), p. 143-175.

Metzger, J. G., Fike, D. A., Osburn, G. R., Guo, C. J., and Aadison, A. N., 2015, The source of gypsum in Mammoth Cave, Kentucky: Geology, 43(2), p. 187-190.

Morehouse, D. F., 1968, Cave development via the sulfuric acid reaction: Bulletin of the National Speleological Society, 30(1), 1-10.

Ono, S., Wing, B., Johnston, D., Farquhar, J., and Rumble, D., 2006, Mass-dependent fractionation of quadruple stable sulfur isotope system as a new tracer of sulfur biogeochemical cycles: Geochimica et Cosmochimica Acta, 70(9), p. 2238-2252.

Plan, L., Tschegg, C., De Waele and J., and Spötl, C., 2012, Corrosion morphology and cave wall alteration in an Alpine sulfuric acid cave (Kraushöhle, Austria): Geomorphology 169, p. 45–54.

Spötl, C., Dublyansky, Y., Koltai, G., Honiat, C., Plan, L., and Angerer, T., 2021, Stable isotope imprint of hypogene speleogenesis: Lessons from Austrian caves: Chemical Geology, 572, 120209.